reviewed paper

Heating with a Novel Type of Retrofitted Thermal Facade Activation and Heat Pump in a Residential Block in Vienna

Constanze Rzihacek, Magdalena Wolf, Thomas Keller, Tobias Pröll

(DI Constanze Rzihacek, BOKU University, Muthgasse 107, 1190 Wien, constanze.rzihacek@boku.ac.at)
(DI Dr. Magdalena Wolf, BOKU University, Muthgasse 107, 1190 Wien, magdalena.wolf@boku.ac.at)
(DI Thomas Keller, BOKU University, Muthgasse 107, 1190 Wien, thomas.keller@boku.ac.at)
(Prof. DI Dr. Tobias Pröll, BOKU University, Muthgasse 107, 1190 Wien, tobias.proell@boku.ac.at)

1 ABSTRACT

Decarbonisation of the building sector is a vital task to cut greenhouse gas emissions and reach Europe's climate targets. This paper presents a novel refurbishment concept which allows the substitution of a fossil-fuelled heating system with a heat pump solution via the addition of a retrofitted thermal activation of the façade for buildings dating from the 1950s and 1960s that can be implemented in full operation of the building. Furthermore, monitoring data from the heating season 2024/25 is used to establish the temporal behaviour of the heat generation system (air-to-water heat pumps), to describe the energy fluxes between various components of the heating system (heat generation, distribution and release), and to evaluate the efficiency of the heating system. The monitoring data used consists of temperature measurement data of the indoor and outdoor environment as well as the heating water flow and return temperatures and façade core temperatures. Additionally, heat meter data for various points in the heating system is used as well as electricity meter data of the heat pumps. Calculated values for amounts of heat generated are cross-validated using heat meter data where available. Results show that in comparison to the available heat meter data, the modelling approach for the thermal power quantification of the heat pumps results in overestimation which would need to be fixed by obtaining more data on the heat pumps' actual efficiency behaviour (COP) for various operating parameters. Finally, the SPF of the heat pumps was established for an observation period of approximately three weeks in January/February 2025 and was found to amount to 3.9.

Keywords: air-to-water heat pump, refurbishment, radiant systems, TABS, efficiency

2 INTRODUCTION

Heating systems using fossil fuels are responsible for approximately 17 % of Austria's greenhouse gas (GHG) emissions [BMK, 2023]. Especially older buildings in their original condition display high heating demands resulting in a higher energy consumption for heating purposes. Thermal refurbishment along with a switch to low-carbon heat generation systems and, if necessary, an adaptation of the heat dissipation systems are therefore key measures to increase the energy efficiency of a building. Especially the extension of existing heat dissipation systems poses a challenge in apartment blocks as access to the flats must be given to conduct the necessary plumbing and building work.

This paper presents a refurbishment concept for apartment blocks with a centralised heating system (one heat generation system for the entire building) that can be executed in full operation of the building and without requiring access to the residents' flats. This refurbishment concept is currently being tested in the course of a dedicated research project (*Sani60ies*, FFG project number 889521) in various test case properties, of which the pilot building located in Große Neugasse (Vienna,IV.) has been in operation and under observation via the monitoring system installed for sufficient time to provide the required data for analysis and evaluation of the heating system's behaviour and efficiency.The refurbishment concept comprises the installation of a hydronic heat dissipation system integrated into the façade from the outside, the thermal refurbishment of the building (thermal insulation applied to the cellar ceiling as well as the attic and the exterior walls) and the substitution of the existing fossil heating system with heat pumps. Details concerning the structure of the façade heating are given in the material and methods section. The measurement data used for the evaluations in this paper was collected during the winter of 2024/2025, during which time the heat generation system consisted of two air-to-water heat pumps at the stated test case building.

In this paper, the behaviour of the heat generation system is analysed by quantifying the amounts of heat produced by the heat pumps as well as the efficiency of the heat pumps in terms of their modelled *COP* and their *SPF* based on measurement data. Additionally, the monitored electrical power data of the heat pumps, the heat meter data as well as the indoor and outdoor air temperatures and the façade core temperature is

used to draw up a heat flow diagram (Sankey diagram) visualising the heat fluxes between the various components in the heating system for a selected time period.

This paper builds on preliminary work prepared for a conference paper for the 2026 IEA Heat Pump Conference (abstract no. 27) which is currently in the submission phase.

3 MATERIAL AND METHODS

The refurbishment concept and, in particular, the design of the façade heating is based on preliminary workespecially by SCHMIDT et al. [2017] and HINTERSEER et al. [2019] who suggest the retrofit of building façades either with capillary mats or multifunctional façade modules containing heating pipes. Further relevant research into radiant systems on a simulation or lab testing basis was conducted by GROß and SCHMIDT [2020], JUNASOVÁ et al. [2022], KRAJČÍK and ŠIKULA [2020], LECIEJ-PIRCZEWSKA and SZAFLIK [2024] and ZOU et al. [2025].

In this section, the case study building and the monitoring system are described and the calculations for the system analysis and evaluation are elucidated.

3.1 Case study building

The case study building is a multi-apartment block dating from 1968 and owned by the social housing association *Sozialbau AG*. It is located in Große Neugasse in Vienna's 4th district and features 2 shops and 20 flats on a conditioned floor area of 1,002 m^2. The building fabric of the external walls consists of *Durisol* bricks which are a mineralised wood wool casing filled with concrete [LEIER, 2024]. The external walls were thermally refurbished and furnished with heating pipes to form an additional heat dissipation system of the building in order to compensate for lowered heating water flow temperatures. These become necessary to ensure an efficient operation of the newly installed heat pumps substituting the old gas boiler. Fig. 1, left shows the structure of the external walls: the heating pipes (raised-temperature-resistant polyethylene pipes) are laid into channels cut into the 2 cm thick exterior render, on top of which the thermal insulation (expanded polystyrene (EPS)) is applied using dowels for fixing. The pipe gap is 30 cm (not to scale in figure). The process of the heating pipes installation is shown in Fig. 1 on the right. In total, the U-value of the exterior walls could be reduced to 0.2 W/m^{2}K instead of 0.93 W/m^{2}K before refurbishment.

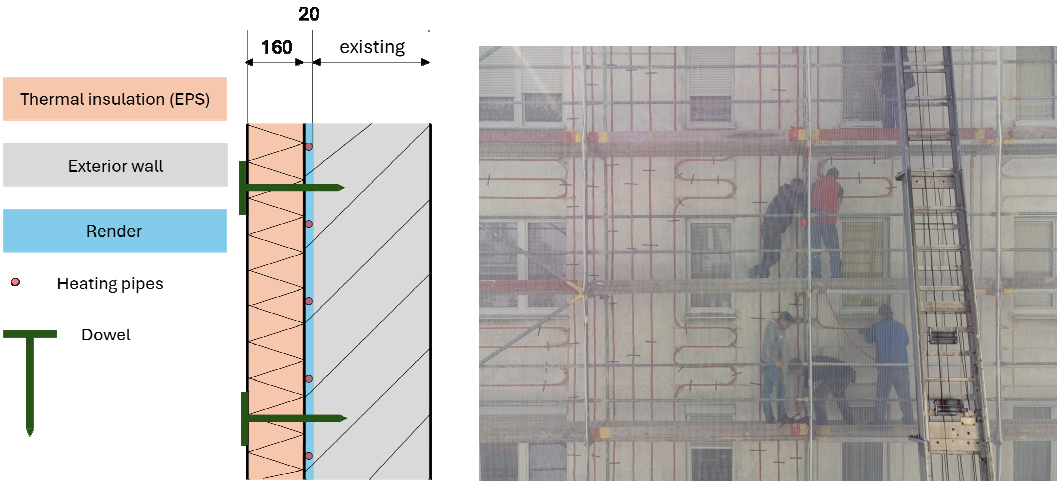

Fig.1: Structure of the external walls after refurbishment (left) and process of installing the heating pipes in the render of the façade before applying the thermal insulation (right).

The heat generation system consists of two *Stiebel Eltron* WPL-A 05 HK 230 Premium air-to-water heat pumps with an EN 14511 rated power of 5 kW at A-7/W35. These supply a buffer tank with 200 l capacity which, in turn, supplies the manifold splitting the heating water to the street and courtyard side heating loops. As indicated above, the façade heating supplements the existing radiator dissipation system. These radiators were still supplied using the gas boiler in the winter 2024/2025 and in operation throughout the heating season.

3.2 Monitoring system

To allow the detailed observation and evaluation of the installed heating system, an elaborate monitoring system was installed measuring the following parameters (all are relevant for the evaluations of this paper with the exception of the heating water flow or return temperature of each heating loop):

- Electrical power of the heat pumps
- Amount of heat transported from the heat pumps to the buffer tank, from the buffer tank to the manifold splitting the heating water into the street and courtyard side supply pipes, amount of heat transported to the street side heating loops and amount of heat transported to the courtyard side heating loops
- Heating water flow and return temperatures between the various system components in the plant room
- Heating water flow or return temperature of each heating loop to supervise presence of a water flow
- Façade core temperature at 5 locations
- Outdoor air temperature
- Indoor air temperature and humidity in one test flat

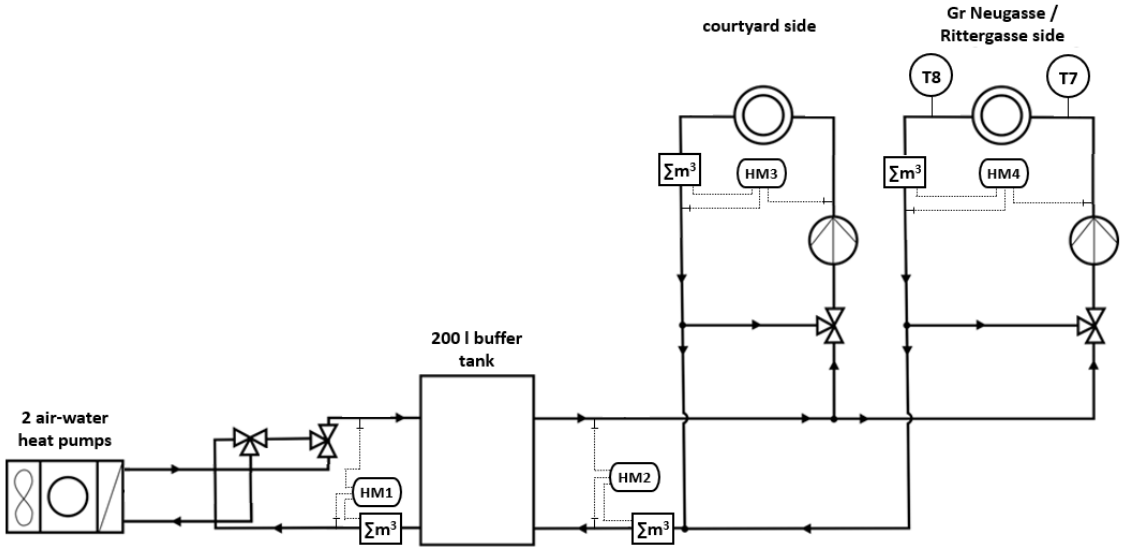

- Fig.2: Position of the heat meters HM1-4 and the PT100 temperature sensors T7 and T8 for the heating water flow and return temperature.

In particular, the electrical power $P_{el,i,j}$of the heat pumps was measured as 5 s mean values using two *Fluke* 1734 three-phase electrical power measurement loggers, the amount of heat transported between heat pumps, buffer tank and manifolds was metered using four *ista* heat meters with ultrasonic transducers and external temperature sensors and the heating water temperatures in the plant room as well as the outdoor air temperature were measured as 15 min mean values using PT100 temperature sensors.The heat meters were read locally at intervals of usually roughly one month. The electrical power loggers provide data for the period from 28th November until 6th December 2024, after which a logging gap due to technical issues with the loggers occurred which lasted until 18th December 2024. From 18th December, the issue was resolved and measurement data was again available until 17th March 2025 which is when the maximum local data storage capacity was reached.At this point, the heating season was, however, practically over due to rising outdoor temperatures. Moreover, as the datalogger collecting the 15 min mean values from the PT100 sensors had some technical issues until 22nd January 2025 resulting in logging gaps, outdoor air temperature data available as 10-minute mean values from *Geosphere Austria* [GEOSPHERE AUSTRIA, 2026] for the weather station "Wien Innere Stadt", ID: 5925 (ca. 600 m linear distance to the test case building) was used for the observation period before the indicated date. Furthermore, the only relevant measurements in the plant room for this paper are the flow and return temperature of the heating water supplied to the façade heating loops. These were only available for the street side heating loops for the winter 2024/2025 as the

sensors used for the courtyard side heating loops were relocated to measure the supply and return temperature of the radiator heating water. For the calculations described below, the heating water flow and return temperature was assumed to be the same for the entire system as both sides are operated to run on the same temperature levels (pumping and mixing units operated accordingly). The position of the heat meters and the temperature sensors measuring the flow and return temperature of the heating water of the street side is shown in Fig. 2.

The façade core temperature is measured using five PT100 temperature sensors which also log 15 minute mean values. Their location in the building façade is shown in Fig. 3.

Fig.3: Position of the façade core temperature sensors (T2-T6, green dots) on the façade in Rittergasse (left) and GroßeNeugasse (right). T1 had to be disconnected to allow the installation of the heating water flow supervision system. The red lines show the heating circuit piping.

The indoor air temperature was measured in one test flat using an *Efento* IoT data logger with a PT1000 temperature sensor. The flat is located on the top floor and looks out on to *Rittergasse* (two top left windows in Fig. 3).

3.3 Calculations

This section details the calculation methods used to establish the *COP* and heat generation of the heat pumps and visualise the heat flow in the heating system for a selected time period using the collected measurement data. Finally, the calculation method for the *SPF* quantification is presented.

3.3.1 Heat generation of the air-to-water heat pumps and COP

The momentary thermal power $\dot{Q}_{th,i,j}$per heat pump*i*per time step *j*was calculated based on their measured electrical power $P_{el,i,j}$and a calculated *COP* depending on the measured heat source (outdoor air) and heat sink (heating water) temperature $T_{source} = T_{out}$and T_{sink}:

$$\dot{Q}_{th,i,j} = P_{el,i,j} \cdot COP \quad [W] \tag{1}$$

Specifically, the*COP*for various heat source and sink conditions was calculated from the information given in the heat pumps' data sheet [STIEBEL ELTRON, s. a.] for the EN 14511 testing points. This was done by establishing the Carnot efficiency $COP_{Carnot}$for each of the three testing points A7/W35, A2/W35 and A-7/W35and then calculating the efficiency factor ζ from the COP_{Carnot} and the stated *COP* in the datasheet per test point by rearranging the following equation to give ζ:

$$COP = COP_{Carnot} \cdot \zeta = \frac{T_{sink}}{T_{sink} - T_{source}} \cdot \zeta \quad [-] \tag{2}$$

where T_{source} is the measured outdoor air temperature (+7, +2 and -7 °C for the test points) and T_{sink} is the setpoint flow temperature of the heating water (35 °C for the test points). The resulting ζ amounted to between 0.47 and 0.49 for the three given test points. Based on this, the *COP* of the heat pumps for other occurring heat sink temperatures was establishedaccording to eq. (2) by calculating the COP_{Carnot} for the three T_{source} of +7, +2 and -7 °C and assumingζ to be constant at 0.47 for all heat sink and source conditions as a worst case scenario. The other occurring setpoint flow temperatureswere determined from the heat pumps' online operation protocol (logbook) logging every change in the heat pumps' setpoints. This was used rather than temperature measurement data from the plant room due to the abovementioned logging gaps of the datalogger used. Fig. 4 shows T_{source} (*Geosphere Austria* data until 23rdJanuary 2025 00:00h and own data since then) and T_{sink} for the period of 1st December 2024 until 31st March 2026.

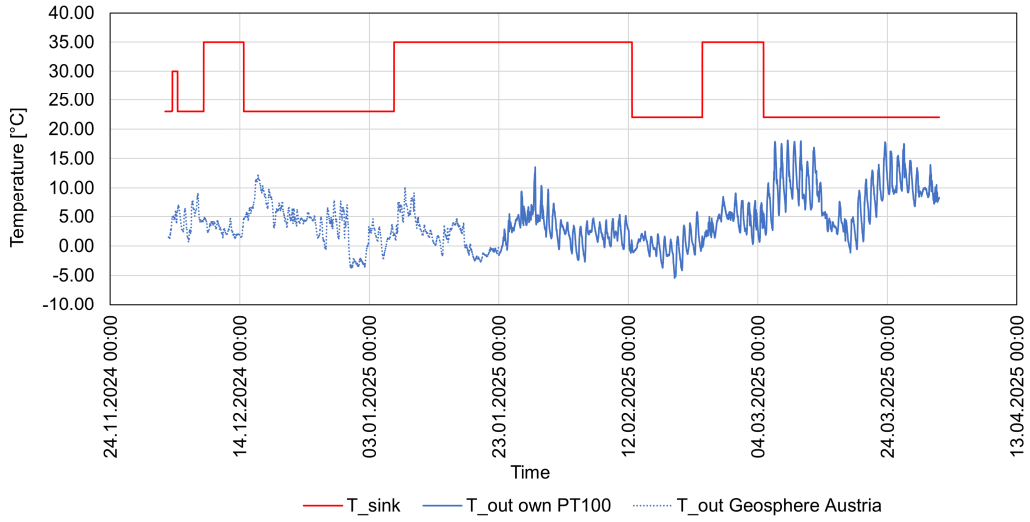

Fig.4: T_{source} (T_{out}) and T_{sink} (heating water setpoint temperature) for the time period from 1st December 2024 until 31st March 2025.

According to the heat pumps' operation protocol and as can largely be seen in Fig. 4, the occurring setpoint flow temperaturesT_{sink} amount to either 35, 30, 23.1, 23 or 22 °C. For every T_{sink}, a polynomial trend function was calculated to describe the *COP* depending on T_{source}= T_{out} (cf. alsoFig. 5 for a visualisation of the trend functions):

$$COP_{35} = 0.0026 \cdot T_{out}^{\ 2} + 0.1407 \cdot T_{out} + 4.3082 \ [-] \quad (3)$$

$$COP_{30} = 0.006 \cdot T_{out}^{\ 2} + 0.1675 \cdot T_{out} + 4.7321 \ [-] \quad (4)$$

$$COP_{23.1} = 0.0136 \cdot T_{out}^{\ 2} + 0.2875 \cdot T_{out} + 5.9727 \ [-] \quad (5)$$

$$COP_{23} = 0.0138 \cdot T_{out}^{\ 2} + 0.2901 \cdot T_{out} + 5.9958 \ [-] \quad (6)$$

$$COP_{22} = 0.016 \cdot T_{out}^{\ 2} + 0.3191 \cdot T_{out} + 6.2374 \ [-] \quad (7)$$

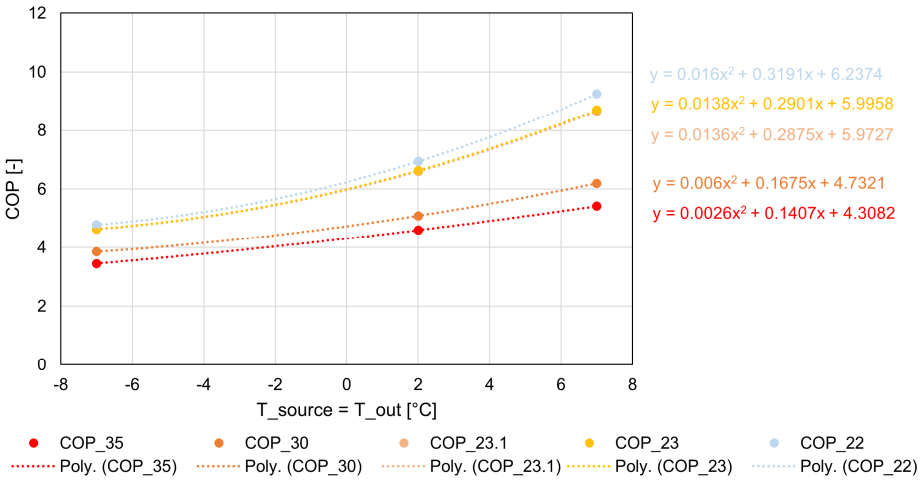

Fig.5: Trend functions of the *COP* for the various heating water flow temperatures T_{sink}.

Thus, for every time step in the evaluated period, the thermal power per heat pump $\dot{Q}_{th,i,j}$ is calculated via eq. (1) using the measured electrical power $P_{el,i,j}$ and the corresponding *COP* function taking in T_{out} according to eqs. (3-7). The amount of heat generated $Q_{th,i,j}$ per heat pump *i* and time step *j*is consequently calculated as:

$$Q_{th,i,j} = \frac{\dot{Q}_{th,i,j} \cdot \Delta t}{3{,}600{,}000} \quad [kWh] \tag{8}$$

where Δt refers to the measuring interval of 5 s. The total amount of heat generated per heat pump *i* is:

$$Q_{th,i,total} = \sum_{j=1}^{n} Q_{th,i,j} \quad [kWh] \tag{9}$$

Thus, the total amount of heat generated by heat pumps 1 and 2 is:

$$Q_{th,total} = Q_{th,1,total} + Q_{th,2,total} \quad [kWh] \tag{10}$$

The calculation of the heat pumps' thermal power and heat generation was conducted for the time period from 6th December 2024 until 17th March 2025. The start date corresponds to the date of the start of the heating mode of the heat pumps and the end date corresponds to the day where the maximum local data storage capacity of the electrical power meters was reached. Due to rising outdoor air temperatures, the heating season was, however, de facto over and the façade heating was operated at very low temperatures (22 °C) until 24th June 2025 which was the day on which the cooling mode for the summer was started. For the calculations of this section, the measurement data not given in 5 s intervals (temperature measurement data) was restructured to match the 5 s intervals of the electrical power measurement data.

3.3.2 Amount of heat transported between the various heating system components

For this, an observation period from 22nd January until 4th February 2025 was chosen as this is a period where all necessary data was available. For the amount of heat generated by the heat pumps, see section 3.3.1. The amount of heat transported to the buffer tank was read from heat meter HM1, see Fig. 2. The difference between the heat generated by the heat pumps and the heat meter data was put down as losses as well as imprecision of the model used to calculate the thermal power of the heat pumps. Furthermore, the heat losses of the buffer tank were calculated as the difference between the amounts of heat measured by the two heat meters on the generation (HM1) and dissipation side (HM2) of the buffer tank. The amount of heat transported to the manifold was calculated as the sum of the amount of heat read from the heat meter metering the courtyard side (HM3) and the amount of heat read from the meter metering the street side (HM4) of the heating circuits. The losses between the buffer tank and the manifold were calculated as the difference in amounts of heat between the buffer tank dissipation side heat meter (HM2) and the manifold (HM3 + HM4). For the last stage in the flow chart, the amount of heat transported to the indoor and outdoor environment ($Q_{facade,in}$and $Q_{facade,out}$) was calculated based on the method employed by SCHNEIDER [2025] for the cooling mode which was adapted here for the heating mode. This method establishes the heat fluxes from the façade heating into the indoor and outdoor environment ($\dot{Q}_{facade,in}$and $\dot{Q}_{facade,out}$) as follows:

$$\dot{Q}_{facade,in} = U_{in} \cdot A_{facade} \cdot \left(\bar{T}_{sys} - T_{in}\right) \quad [W] \tag{11}$$

$$\dot{Q}_{facade,out} = U_{out} \cdot A_{facade} \cdot \left(\bar{T}_{sys} - T_{out}\right) \quad [W] \tag{12}$$

where U_{in} and U_{out} refer to the U-value of the wall layers between façade heating pipes and indoor or outdoor environment of 0.97 W/m^{2}K and 0.25 W/m^{2}K, respectively.A_{facade} refers to the activated façade area of 569.6 m^2, T_{in} and T_{out} to the indoor and outdoor air temperature and $\bar{T}_{sys}$ to the mean system temperature of the façade heating which was calculated as:

$$\bar{T}_{sys} = \frac{T_{flow,GrNeu} + T_{return,GrNeu} + \bar{T}_{facade}}{3} \quad [°C] \tag{13}$$

where $T_{flow,GrNeu}$and $T_{return,GrNeu}$ refer to the flow and return temperature of the façade heating measured by T7 and T8 in Fig. 2 and $\bar{T}_{facade}$ to the mean façade core temperature calculated as the arithmetic mean of the temperature measured by the five PT100 sensors shown in Fig. 3:

$$\bar{T}_{facade} = \frac{\sum_{i=1}^{n} T_{facade,i}}{n} \quad [°C] \tag{14}$$

Where $T_{facade,i}$ is the temperature measured by the sensor i and n is the total number of sensors = 5. The amount of heat transported was calculated from the heat fluxes $\dot{Q}_{facade,in}$and $\dot{Q}_{facade,out}$ similarly to eq. (8):

$$Q_{facade,in} = \frac{\dot{Q}_{facade,in} \cdot \Delta t}{3{,}600{,}000} \quad [kWh] \tag{15}$$

$$Q_{facade,out} = \frac{\dot{Q}_{facade,out} \cdot \Delta t}{3{,}600{,}000} \quad [kWh] \tag{16}$$

with Δt as the time step of 15 minutes, i.e. 900 s. Finally, the difference between the heat metered by HM3 + HM4 in comparison to $Q_{facade,in}$ + $Q_{facade,out}$ was put down as losses as well as inaccuracies of the heat dissipation modelling.

3.3.3 SPF calculation

The *SPF* was established for the time period of 10th January until 4th February 2025. This is the longest heat meter reading interval with full availability of electrical power measurement data. The best available measured heat data for the heat pumps' thermal production is that logged by HM1 between the heat pump and the buffer tank inlet. The *SPF* was thus calculated as follows:

$$SPF = \frac{heat\ \text{transported}\ measured\ by\ heat\ meter\ \text{HM1}}{E_{el,total}} \quad [-] \tag{17}$$

where $E_{el,total}$ refers to the total electricity consumption of heat pumps 1 and 2:

$$E_{el,total} = E_{el,1,total} + E_{el,2,total} \quad [kWh] \tag{18}$$

which, in turn, are calculated as:

$$E_{el,i,total} = \sum_{j=1}^{n} E_{el,i,j} \quad [kWh] \tag{19}$$

Finally, the electrical power consumption per heat pump i and time step j is calculated as:

$$E_{el,i,j} = \frac{P_{el,i,j} \cdot \Delta t}{3{,}600{,}000} \quad [kWh] \tag{20}$$

With $P_{el,i,j}$as the mean power consumption of heat pump i in the time step j and Δt as the logging interval of 5 s.

4 RESULTS AND DISCUSSION

First, the results for the heat pumps' thermal power as well as heat production are presented along with the trajectory of their momentary *COP*. Then, the results of the heat flow analysis for the time period from 22nd January until 4th February are elucidated. Finally, the *SPF* resulting for the time period of 10th January until 4th February 2025 is presented.

4.1 Heat generation of the air-to-water heat pumps andCOP

The momentary thermal power$\dot{Q}_{th,i,j}$ as well as the cumulative heat produced $Q_{th,i,total}$per heat pump are shown in Fig. 6.

As can be observed, the thermal power of the heat pumps is reduced during periods of lower heating water setpoint temperatures, such as from 14th December 2024 until 6th January 2025 or from 12th until 23rd February 2025 where the setpoint temperature amounted to 23 and 22 °C, respectively. Furthermore, the prioritisation of heat pump 2 can be observed from the data in that heat pump 1 remains inactive during periods with lower demand. The prominent spikes in the momentary thermal power especially evident from 4th March 2025 are due to the reduction of the setpoint flow temperature to 22 °C at that date together with outdoor air temperatures rising to levels permanently above 5 °C and reaching upto 18 °C, resulting in a very high *COP*; see Fig. 7. The total calculated amount of heat generated during the entire observed timespan $Q_{th,total}$amounts to 15,028 kWh. Comparing this roughly to the amount of heat metered by the heat meter located between heat pumps and buffer tank (HM1) during the period of 6th December 2024 until 25th March

2025 of 13,543 kWh, a not inconsiderable discrepancy emerges, especially taking into account the logging gaps of the electrical power meters which, if filled, would result in even higher calculated amounts of heat.

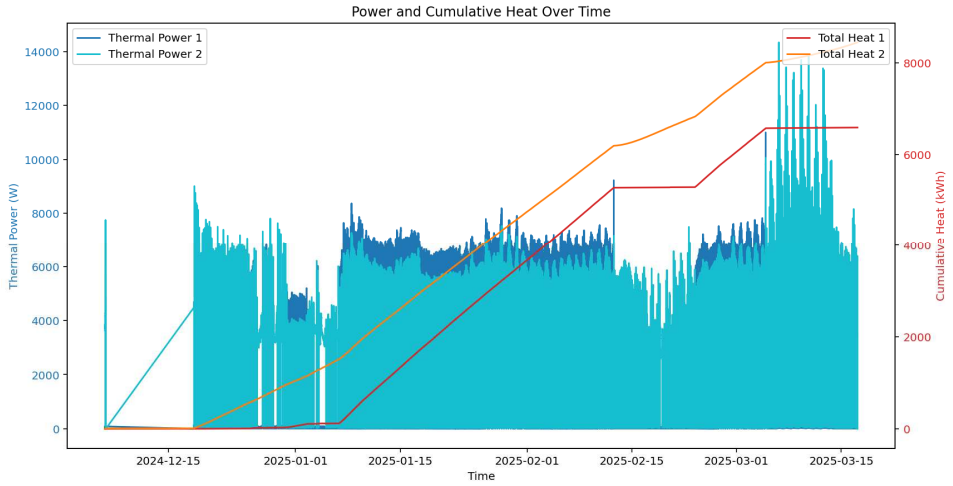

Fig.6: The thermal power provided $Q_{th,i,j}$ and cumulative heat generated $Q_{th,i,total}$ per heat pump for the timespan from 6th December 2024 until 17th March 2025.

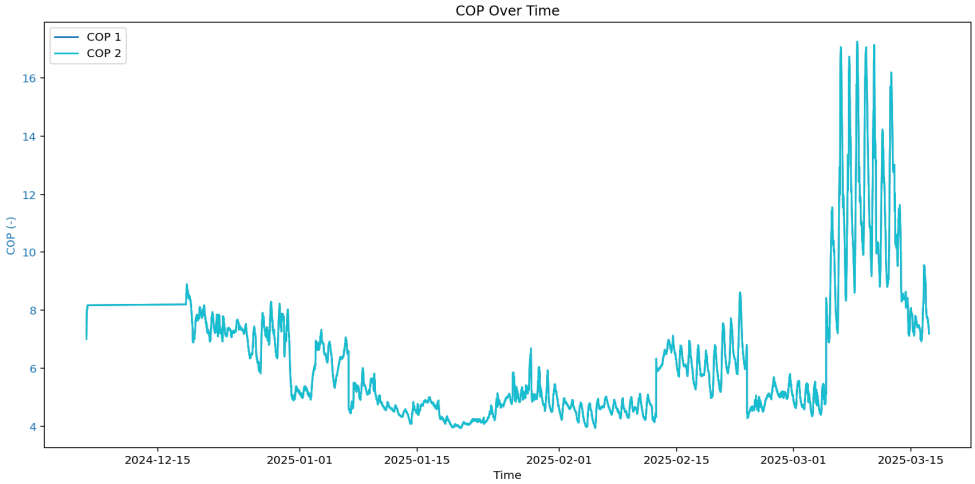

Fig. 7: The *COP* of the heat pumps for the time period from 6th December 2024 until 17th March 2025.

To give a clearer picture, a shorter time period according to a heat reading interval with full availability of electrical power data was selected and the amount of heat generated calculated. This is the period from 22nd January until 4th February 2025. The results are shown in Fig. 8.

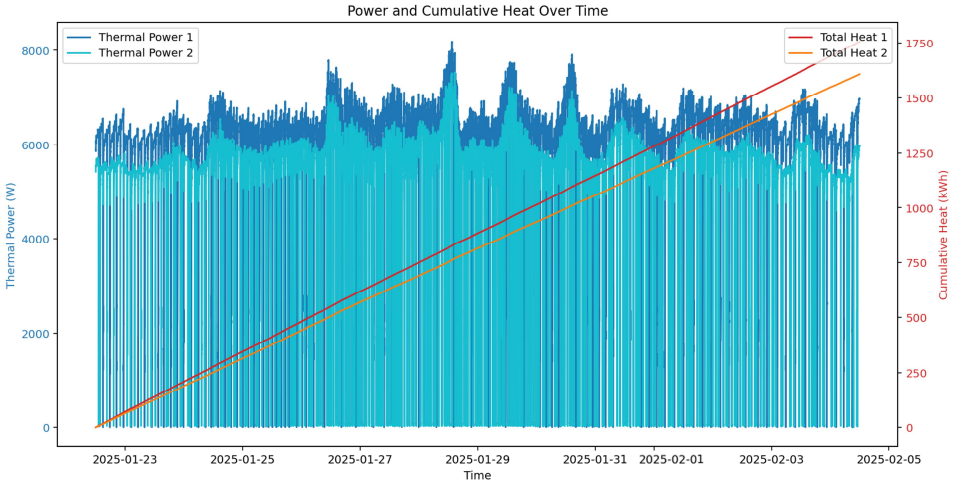

Fig.8: The thermal power provided $Q_{th,i,j}$ and cumulative heat generated $Q_{th,i,total}$ per heat pump for the timespan from 22nd January until 4th February 2025.

During this period, the heating water setpoint temperature amounted to 35 °C and the outdoor air temperature fluctuated between -2 °C and +13 °C.The *COP* fluctuated between 4 and 6.7, see Fig. 9.

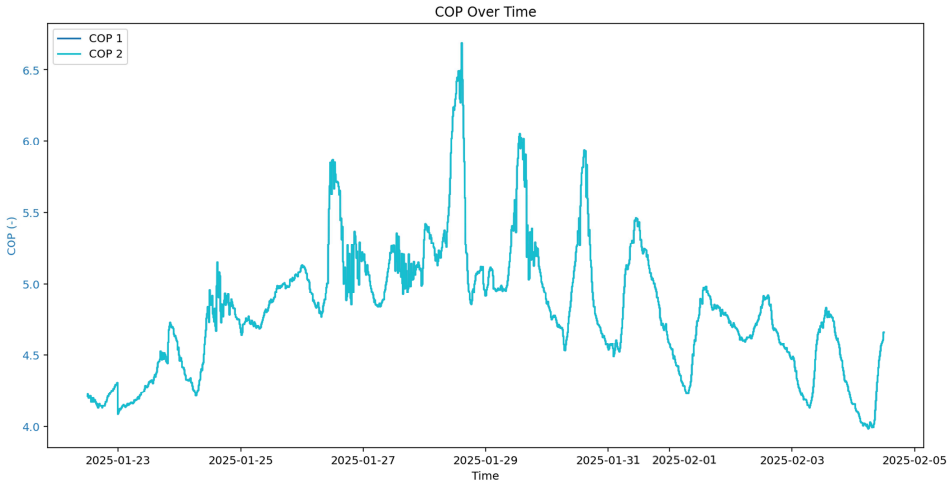

Fig. 9: The *COP* of the heat pumps for the time period from 22nd January until 4th February 2025.

During this period, the total amount of calculated heat amounts to 3,365 kWh and the amount of heat metered between heat pumps and buffer tank by HM1 to 3,142 kWh. Naturally, a certain amount of heat will be lost during transport from the heat pumps to HM1; however, as will be shown in the following section, heat losses in the buffer tank and piping are quite low for other components. A certain inaccuracy of the model must therefore be inferred.

4.2 Amount of heat transported between the various heating system components

To give a clearer picture of the amount of heat transported in the heating system, the timespan from 22nd January until 4th February 2025 with full monitoring data availability (temperature logging, heat metering and electrical power logging) was selected to visualise the observed and calculated energy fluxes. The results are shown in Fig. 10.

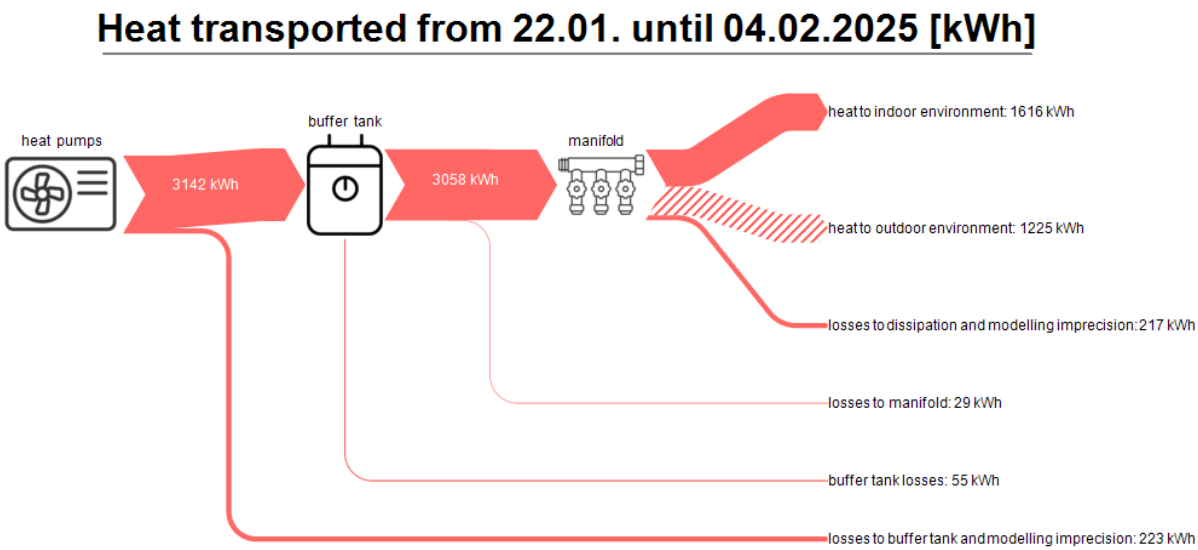

Fig. 10: Flow chart showing the measured and calculated amounts of heat transported between the various heating system components for the timespan from 22nd January until 4th February 2025.

This shows that of the 3,365 kWh produced by the heat pumps, 1,616 kWh (48 %) are supplied directly to the indoor environment and 1,225 kWh (36 %) are lost to the outdoor environment. However, the total amount of heat released via the façade activation of 2,841 kWh (84 %) contributes to the formation of a thermal barrier between indoor and outdoor environment and thus inhibits a potential heat flux from the indoor environment to the outdoor environment as long as the façade core temperature is higher than or close to the indoor air temperature. Thus, the heat flux from the façade to the outdoor environment is the price we pay for the formation of the thermal barrier. The heat losses of the buffer tank as well as of the piping

between buffer tank and manifold are relatively low which implies that the losses observed between the heat pumps and buffer tank as well as the manifold and the heat dissipation system (façade activation) are not entirely due to real losses in the piping, but also to inaccuracies of the models used to calculate the heat pumps' heat production as well as the heat release by the façade. The larger portion of the discrepancy at the heat generation end is very likely due to model inaccuracies as the pipe length between heat pumps and heat meter is rather short; however, the discrepancy at the dissipation end could indeed be mainly due to losses in the piping as the heating water travels some distance from the manifold in the plant room to the supply string at the bottom of the façade from which the individual heating circuits branch off. Various factors are likely to contribute to inaccuracies in the models used: apart from measurement errors, the assumptions made for the calculations are a source of inaccuracy. For the heat pumps' thermal power modelling, the estimation of the *COP* via the Carnot efficiency and an assumed constant ζ is, of course, a less accurate method than measured *COP* data for a larger number of testing points. Pertaining to this, also the assumption of a polynomial relationship between *COP* and heat source temperature could be questioned. For the façade heating's heat release calculation, the assumption of a uniform indoor air temperature in the entire building based on the measurement data for the only available indoor air temperature measurement device may not be representative for the entire building. Similarly, the assumption of the applicability of the heating water flow and return temperatures of the street side heating circuits to the courtyard side heating circuits must be borne in mind when interpreting the results. Overall, the largest source of inaccuracy seems to be the calculated *COP* which results in an overestimation of the thermal production of the heat pumps. This could best be rectified by establishing the behaviour of the heat pumps' efficiency via dedicated measurements.

4.3 SPF calculation

For the period of 10th January until 4th February 2025, a total amount of electricity consumed of 1,437 kWh in comparison to a measured amount of heat of 5,657 kWh was observed, resulting in a *SPF* of 3.9. This seems an acceptable *SPF* for the given heat source and heat sink conditions [ŠIMKO et al., 2024]. A slight inaccuracy in this calculation is caused by the positioning of the heat meter measuring the amount of generated heat (HM1). This is situated on the supply side of the buffer tank. Heat losses occurring in the piping between the heat pumps and the heat meter are therefore expected to result in slightly smaller amounts of measured heat than that produced by the heat pumps. However, these losses are expected to be small and bear a small significance to the *SPF* calculated.

5 CONCLUSION

In conclusion, the calculated *COP* fluctuates largely between 4 and 9 between 6th December 2024 and 17th March 2025 (with the exception of the outliers towards the end of the observation period with values of up to 17). The calculated total amount of heat generated amounts to 15,028 kWh, however, a comparison of this value to the heat meter data implies that the model overestimates the thermal power and heat production of the heat pumps. A more limited time period from 22nd January until 4th February 2025 with full availability of measurement data is chosen to evaluate the modelling approaches more closely and visualise the heat fluxes occurring between the various heating system components. It is found that the chosen modelling approach indeed overestimates the heat production of the heat pumps. The approach employed for the quantification of the heat fluxes directed from the façade heating to the indoor and outdoor environment appears to be more accurate. To counteract the thermal power overestimation, more information concerning the actual *COP* behaviour of the heat pumps would be necessary. In terms of the useful energy transported in the heating system, 48 % of the heat generated is released to the indoor environment and 36 % of the heat is lost to the outdoor environment. In terms of the total efficiency of the heat generation system, the *SPF* of the heat pumps amounts to 3.9for the period from 10th January until 4th February 2025.

6 REFERENCES

BMK – BUNDESMINISTERIUM FÜR KLIMASCHUTZ, UMWELT, ENERGIE, MOBILITÄT, INNOVATION UND TECHNOLOGIE: Der Beitrag von Wärmepumpen zur Wärmewende. Unterlage zum Branchentreff am 04. Juli 2023. Wien, 2023. URL:https://www.bmwet.gv.at/dam/jcr:e3b0224b-8f31-4274-97ef-57157cdf2e3d/BMK_Der%20Beitrag%20von%20W%C3%A4rmepumpen%20zur%20W%C3%A4rmewende%20-%20Unterlage%20zum%20Branchentreff.pdf [last accessed on 08.01.2025 at 14:20h].

GEOSPHERE AUSTRIA: Messstationen Zehnminutendaten v2. Dataset for the weather station ‚Wien Innere Stadt', ID: 5925. Vienna, 2026. URL: https://dataset.api.hub.geosphere.at/app/frontend/station/historical/klima-v2-10min [last accessed on 07.01.2026 at 11:50h].

GROß, Bodo and SCHMIDT, Christoph: Schlussbericht zum Vorhaben: „LEXU II – Low ExergyUtilisation – Einsatz von außenliegender Wandtemperierung – Feldtest CO2-Wärmepumpe mit Eisspeicher".Saarbrücken: IZES gGmbH, 2020. URL: https://www.tib.eu/en/search?tx_tibsearch_search%5Baction%5D=download&tx_tibsearch_search%5Bcontroller%5D=Download&tx_tibsearch_search%5Bdocid%5D=TIBKAT%3A1733879153&cHash=ff97b23ce505c76bfc5a2c0070ed1a52#download-mark[last accessed on 26.02.2026 at 11:00h].

HINTERSEER, Simon; NEUSSER, Maximilian; BEDNAR, Thomas; HUBER, Hermann; SCHNABEL, Thomas; PORTUGALLER, Benjamin; LEEB, Markus; KARNUTSCH, Markus; GNIGLER, Matthias and REITER, Thomas: Forschungsbericht Smart Skin – Salzburger Multifunktionsfassade. Wien, Salzburg: TU Wien, FH Salzburg, 2019. URL: https://www.fh-salzburg.ac.at/fileadmin/fhs_daten/studiengaenge/smb-smc/documents/SMB_publication2019.pdf[last accessed on 26.02.2026 at 14:15h].

JUNASOVÁ, Barbora; KRAJČÍK, Michal; ŠIKULA, Ondřej; ARICI, Müslüm and ŠIMKO, Martin: Adapting the construction of radiant heating and cooling systems for building retrofit. Energy & Buildings 268: Art. Nr. 112228. 2022. DOI: https://doi.org/10.1016/j.enbuild.2022.112228.

KRAJČÍK, Michal and ŠIKULA, Ondřej: The possibilities and limitations of using radiant wall cooling in new and retrofitted existing buildings. Applied Thermal Engineering 164: Art. Nr. 114490.2020. DOI: https://doi.org/10.1016/j.applthermaleng.2019.114490.

LECIEJ-PIRCZEWSKA, Dorota and SZAFLIK, Władysław: Heat Flow Through a Wall with a Thermal Barrier. Advances in Science and Technology Research Journal 18(5); pp. 277-286. 2024. DOI: https://doi.org/10.12913/22998624/190474.

LEIER = LEIER BAUSTOFFE GMBH UND CO KG: Durisol DMI 25/18. Datasheet. S. l., 2024. URL: https://www.leier.at/wp-content/uploads/2024/11/PDB-Durisol-DMI-25 18.pdf?x98573 [last accessed on 13.01.2025 at 14:45h].

SCHMIDT, Christoph; LUTHER, Gerhard; ALTGELD, Horst; MAAS, Stefan; GROß, Bodo and SCHOLZEN, Frank: „Außenliegende Wandtemperierung" – LowEx-Anwendung zur Temperierung von Bestandsgebäuden und thermischen Aktivierung der Bestandswand: theoretische Grundlagen und Kennwerte. Bauphysik 39(4): pp. 215 223. 2017. DOI: https://doi.org/10.1002/bapi.201710028.

SCHNEIDER, Konrad Christian: Thermische Fassadenaktivierung im Bestand: Messtechnische Evaluierung eines aktivierten Systems. Master Thesis submitted at BOKU University. Vienna, 2025.

ŠIMKO, Martin; PETRÁŠ, Dušan; SZABÓ, Daniel; ŽIVNER, Lukášand TAKÁCS, Ján: Testing the Efficiency of a Heat Pump with Radiant Systems in Heating Mode. PeriodicaPolytechnica Mechanical Engineering 68(4): pp. 320-327. 2024.

STIEBEL ELTRON: TechnischesDatenblatt. WPL-A 05 HK 230 Premium Luft-Wasser-Wärmepumpen. S.l., s. a. URL: https://www.stiebel-eltron.at/de/home/produkte-loesungen/erneuerbare_energien/waermepumpe/luft-wasser-waermepumpen/wpl-a-05 07-hk-premium/wpl-a-05 hk-230-premium/technische-daten.product.pdf [last accessed on 12.01.2026 at 15:20h].

ZOU, Huajun; CHAI, Ruiwen; CHEN, Zhiqiang; LI, Shuying; BAO, Xuefang; CHEN, Sarula; CHEN, Kunyu and YANG, Yang: Thermal Performance and Energy Efficiency Evaluation of Thermally Activated Composite Panel for Retrofitted Buildings Across Diverse Climate Zones of Gansu, China. Buildings 15(20): Art. Nr. 3763. 2025. DOI: https://doi.org/10.3390/buildings15203763.